Dynamics of viscous liquid bridges inside microchannels subject to external oscillatory flow

Majid Ahmadlouydarab, Jalel Azaiez, and Zhangxin Chen
Department of Chemical and Petroleum Engineering, Schulich School of Engineering, University of Calgary, Calgary, Alberta, Canada T2N 1N4

(Received 6 May 2014; published 2 February 2015)

We report on two-dimensional simulations of liquid bridges' dynamics inside microchannels of uniform wettability and subject to an external oscillatory flow rate. The oscillatory flow results in a zero net flow rate and its effects are compared to those of a stationary system. To handle the three phase contact lines motion, Cahn-Hilliard diffuse-interface formulation was used and the flow equations were solved using the finite element method with adaptively refined unstructured grids. The results indicate that the liquid bridge responds in three different ways depending on the substrate wettability properties and the frequency of the oscillatory flow. In particular below a critical frequency, the liquid bridge will rupture when the channel walls are philic or detach from the surface when they are phobic. However, at high frequencies, the liquid bridge shows a perpetual periodic oscillatory motion for both philic and phobic surfaces. Furthermore, an increase in the frequency of the flow velocity results in stabilization effects and a behavior approaching that of the stationary system where no rupture or detachment can be observed. This stable behavior is the direct result of less deformation of the liquid bridge due to the fast flow direction change and motion of contact lines on the solid substrate. Moreover, it was found that the flow velocity is out of phase with the footprint and throat lengths and that the latter two also show a phase difference. These differences were explained in terms of the motion of the two contact lines on the solid substrates and the deformation of the two fluid-fluid interfaces.

DOI: 10.1103/PhysRevE.91.023002 PACS number(s): 47.55.nk

I. INTRODUCTION

The behavior of liquid or capillary bridges has received a lot of attention given their importance in a wide range of natural and industrial applications. These include enhanced oil recovery, water removal management in proton exchange membrane fuel cells (PEMFC), coating of liquid films on solids, pigments dispersion, particles agglomeration and sedimentation, microgravity applications, multiphase flows, and phase change such as evaporation and condensation in porous media [1–7]. Since in most of these applications the volume and dimensions of the liquid bridge are rather small, gravitational and inertial forces do not play significant roles in determining its shape, and surface forces are the dominant factors [8,9].

Existing studies can be classified under two categories. The first one deals with stationary systems in the absence of external flow effects. For this category, stretching, squeezing, slipping, spreading, spinning, and oscillation of liquid bridges between parallel or tilted plates, spheres, or combinations of spheres or particles and plates have been the subject of numerous analytical, numerical, and experimental studies that span many decades [3,4,10–14]. Up to the 1980s, most studies have focused on the equilibrium shapes of the bridges and their stability. These studies have addressed situations in which an axisymmetric liquid bridge is held between two parallel and axially aligned circular disks of equal radii in the absence as well as in the presence of gravity [15–17]. The main objectives of most of these studies were to obtain the magnitude of the forces acting on the bridge in stationary or equilibrium states, or determine the durability of the liquid bridge under stretching, squeezing, spinning, or axial and nonaxial vibration between solid disks [16,18–22].

In particular, Xhang *et al.* [11] conducted experimental and numerical studies to determine the nonlinear dynamics of an axisymmetric liquid bridge between two coaxial, circular, solid disks that are pulled apart at a constant velocity. It was found that as the disks were continuously pulled apart, the bridge deforms and ultimately breaks up, leaving two drops on the two disks. They analyzed the effects of various physical properties such as viscosity, and geometrical properties such as the gap size on the liquid bridge deformation and rupturing. In a later study, Meurisse and Querry [5] adopted a theoretical analytical model to determine the normal forces on parallel solid plates when squeezing a flat liquid bridge. Their model took into account the hydrodynamic (viscous dissipation) and the capillary effects as well as the evolution of the geometry of the liquid bridge with time. Specifically in this category, the response of the liquid bridge to high-frequency axial vibrations of the disks has been investigated. The disk vibration causes surface oscillations as well as mean flow because of the generation of a mean vorticity in the viscous boundary layer near the disks and surface wave propagation at the liquid bridge free surfaces [23]. The effect of vibrations applied to a captive liquid bridge in nonaxial directions (parallel to the disks) also has been studied numerically and experimentally [22,24]. Results indicated that the liquid bridge surface could be more sensitive to transverse accelerations normal to the liquid bridge surface. It should be noted that the authors did not report the existence of any mean flow in nonaxial vibration, at least in the range of parameters they adopted. More recently in a 3D computational research, Ru-Quan and Kawaji reported only the existence of the transversal vortices inside the liquid bridge when a horizontal vibration was applied [25].

The second category of studies focused on the physics of the system in the presence of an external flow. In particular, the dynamics of liquid bridges under constant external flow rates between parallel plates, tubes, and in a disordered media such as a porous medium [9,26–28]. For example,

Gunstensen and Rothman [26] analyzed immiscible two phase flows in porous media using the lattice-Boltzmann technique. The porous medium was initially occupied by one of the phases, then through an increase in the flow rate of the other phase, rupturing of liquid bridges and different types of flow regimes were identified. In another numerical analysis, Ahmadlouydarab *et al.* [29] studied the behavior of the liquid bridge inside corrugated microchannels in the presence of a steady external flow. They concluded that the competition between the capillary forces and the external flow induced forces and that liquid bridge volume and channel geometry are the determinant factors to observe different responses from liquid bridge including detachment and rupturing.

All existing studies have focused on either stationary liquid bridges captive between plates or particles or situations where the bridge is displaced under steady flow rate inside channels or between plates. We examine here the effects of oscillatory external flows on the behavior and stability of liquid bridges, without any constraint, inside confined pathways where liquid bridge can easily move, fluctuate, deform, rupture, and/or detach from the walls.

The lack of studies on liquid bridge's behavior in confined pathways motivated the present work which has two main objectives. First, we will try to understand the dynamics of a located liquid bridge inside a 2D straight microchannel and subject to a pure oscillatory flow (zero net flow). As such, the physics of the present system are different from those of the axisymmetric liquid bridge, already found in the literature. Second, we will explore whether the liquid bridge response and external flow are in the same phase or not and how to rationalize it if so. It will be assumed that the microchannel walls have uniform and identical wettability properties. Using a diffuse-interface model to handle the motion of the contact lines and the finite element method accompanied with adaptive unstructured grid, a systematic analysis of the flow is conducted. The effects of the flow rate frequency as well as the wall wettability on the liquid bridge morphology are analyzed and the response of the bridge to the flow is characterized by examining the variations of the footprint and throat lengths. In addition to these two quantitative parameters, development of the interfacial morphology of the liquid bridge in time is used to understand the physics in depth.

The results of this study are relevant to processes that involve time-dependent flows encountered, for example, in conventional applications such as enhanced oil recovery as well as in modern ones such as microfluidics, and laboratory-on chips devices.

II. PROBLEM SETUP AND METHODOLOGY

A. Computational domain characteristics

As we are interested in 2D calculations, a computational domain consisting of a rectilinear channel with a liquid bridge located at the center is considered. The top and bottom walls are assumed to have uniform and identical wettability properties, which allows one to limit the analysis to only half of the physical domain. The 2D symmetric-planar geometry, with a rectangular computational domain of length L and height H including the liquid bridge of width W, is shown in Fig. 1. The liquid bridge is assumed to initially have a rectilinear shape. Such a shape is not at equilibrium except for an initial contact angle of $\pi/2$. Furthermore, it is assumed that both the liquid bridge and the surrounding fluid are initially at rest. As soon as the computation starts and the liquid bridge makes contact with the substrate, it adjusts to the local contact angles, deforms, and depending on the applied conditions, it may start to move and fluctuate inside the microchannel. Physically this can be considered to represent a cuboid liquid bridge of width W, height $2H$, and infinite depth, which is trapped inside a microchannel of infinite depth. It is important to choose W in a way that without imposing external flow, the liquid bridge neither ruptures nor detaches as a result of the wall wettability. For example, inside a microchannel with philic walls and based on our derived equation (9), the throat thickness has to be larger than zero.

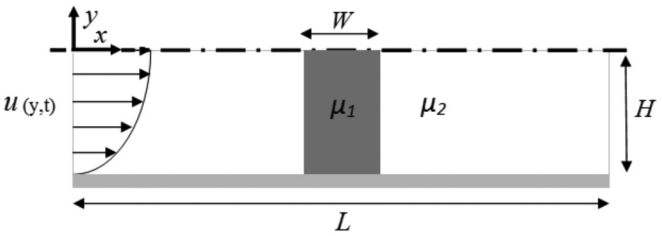

$$u(y,t) = u_{max}(1-(\frac{y}{H})^2)cos(2\pi Ft)$$

FIG. 1. Schematic of the initial configuration for 2D symmetric-planar computations at a time $t = 0$. The expression of the pure oscillatory flow's velocity with a zero average over a period is shown.

B. Methodology and governing equations

In the system which consists of a microchannel and liquid bridge of microsizes, gravitational and inertial forces are negligible; hence such a system can be modeled using Stokes equations. Furthermore, since the system involves the deformation and movement of interfaces, three-phase contact lines, and surface wettability, a diffuse-interface formulation with the Cahn-Hilliard model is adopted to handle the generated singularity as an alternative approach. Using Cahn-Hilliard diffusion is a convenient way for capturing the interfacial deformation and regularizing the interfacial jump as well as the contact-line singularity [30–32].

A phase-field variable ϕ is introduced such that $\phi = 1$ in one fluid and $\phi = -1$ in the other. The two-phase flow is described by the modified stokes and Cahn-Hilliard equations:

$$\nabla \cdot u = 0, \tag{1}$$

$$\nabla p = \nabla \cdot [\mu(\nabla u + \nabla u^{\mathrm{T}})] + Q\nabla\phi, \tag{2}$$

$$\frac{\partial \phi}{\partial t} + u \cdot \nabla\phi = m\nabla^2 Q, \tag{3}$$

where m is the Cahn-Hilliard mobility, $Q = \lambda[-\nabla^2\phi + \frac{\phi(\phi^2-1)}{\epsilon^2}]$ is the chemical potential, and $Q\nabla\phi$ is the diffuse-interface representation of the interfacial tension. The two parameters λ and ϵ are the interfacial energy density and the

capillary width of the interface, respectively, and their ratio $\sigma = \frac{2\sqrt{2}}{3}\frac{\lambda}{\epsilon}$ gives the interfacial tension in the limit of sharp interfaces [32]. The effective viscosity μ represents the average of those of the two fluids weighted by their volume fractions, $(1+\phi)/2$ and $(1-\phi)/2$. This viscosity varies sharply but continuously across the interface between those of the liquid bridge μ_1 and surrounding fluid μ_2. In this case, the gas-liquid interface is no longer a boundary that requires boundary conditions [32].

It is difficult to choose a velocity profile on the left and right side of the domain when considering oscillatory multiphase flows [33,34]. It is however expected that the effects of the velocity profile on the results can be reduced by choosing long channels. Existing literature suggests that in oscillatory stokes flow of a single phase, the entrance length, L_e, becomes as large as in steady single phase flow [34,35]. On the other hand, Chen [36] suggested $L_e/D = 0.315$ for stokes flow in 2D channels or between parallel plates. This was similar to what was given by Atkinson *et al.* [37]. Based on these, we have located the liquid bridge center at $2.5W$ far from both inlet and outlet. Given the height of the channel W, this results in a ratio of 2.5 which is very large compared to 0.315. Also it is assumed that the tangential component of the velocity is zero at the left and right sides of the domain and a time-dependent velocity profile is considered for the normal component as follows:

$$u(y,t) = u_{\max}\left[1 - \left(\frac{y}{H}\right)^2\right]\cos(2\pi Ft), \tag{4}$$

where F is the frequency. Note that the net injection flow over a period is zero ($\overline{u} = 0$) and the discussion will be centered around the effects of the characteristics of this oscillatory profile and comparisons with the stationary system $u = 0$.

On the solid substrate, the following boundary conditions are used:

$$u = 0, \tag{5}$$

$$n \cdot \nabla Q = 0, \tag{6}$$

$$\lambda n \cdot \nabla\phi + f_w'(\phi) = 0, \tag{7}$$

where n is the normal vector pointing into the wall and $f_w(\phi) = -\sigma\cos\theta\frac{\phi(3-\phi^2)}{4}$ is a wall energy [38,39]. Equation (5) imposes no slip on the substrate, and the contact line motion is achieved via Cahn-Hilliard diffusion. Equation (6) implies no penetration of the fluid components into the wall. Equation (7) is a natural boundary condition that follows from the variation of the wall energy, and specifies the local contact angle θ [38]. Furthermore, since only half of the physical domain is considered, symmetric conditions are applied at the top boundary of the computational domain. Finally, periodic boundary conditions are imposed at the left and right ends of the domain.

C. Dimensionless groups

The dimensionless parameters of the problem include the geometrical length ratios $H_W = H/W$ and $L_W = L/W$, the viscosity ratio of the liquid bridge to the surrounding fluid $M = \mu_1/\mu_2$, the solid substrate contact angle θ, the maximum capillary number $\mathrm{Ca}_{\max} = \mu_1 u_{\max}/\sigma$, and the dimensionless frequency $f = F\mu_1 W/\sigma$. The last two dimensionless parameters come from the oscillatory flow rate. The dimensionless form of the velocity at the domain's boundaries is $\tilde{\mathrm{Ca}} = \mathrm{Ca}_{\max}[1-(\frac{y}{H})^2]\cos(2\pi ft)$, where the dimensionless time is defined as $t = t^*\sigma/(\mu_1 W)$. The spatial average capillary number on the boundaries is defined as $\mathrm{Ca} = \frac{\int \tilde{\mathrm{Ca}}\,dy}{W}$ with a zero average over a period $\overline{\mathrm{Ca}} = 0$. In the remainder the star superscripts are dropped from all dimensionless quantities. Furthermore, the Cahn-Hilliard model introduces two mesoscopic dimensionless parameters: the Cahn number $Cn = \epsilon/W$ and the diffusion parameter $\Lambda = l_d/W$. The former is the ratio between the interfacial thickness and the macroscopic length, while the latter is between the *diffusion length* $l_d = (\mu_1\mu_2)^{1/4}m^{1/2}$ and W. There are several interesting questions about the Cahn-Hilliard model on how to choose related parameters. These questions have been extensively examined in numerous studies [39–42]. However, it is worth mentioning that these parameters must be chosen judiciously, and in particular Cn should be small enough for the sharp-interface limit to be approached [32,43]. Furthermore, l_d is the counterpart of the *slip length*, l_s commonly used in sharp-interface models [38,39,44], and Λ represents the strength of Cahn-Hilliard diffusion in moving the contact line, and is closely related to the contact line speed. Thus it should in principle be determined by fitting an experimental datum for the specific fluids and substrate material [39]. In this study it was found that reducing Cn from large values to 10^{-2} and choosing $\Lambda = 10^{-2}$ allows one to reach the sharp interface limit. Detailed comparison with literature and validation are presented in the following section.

The model equations are solved using the Galerkin finite-element method on a triangular grid, with an implicit time-marching scheme and Newton iterations at each time step. The grids near the fluid interface are adaptively refined and coarsened as the interface moves. The theoretical model and numerical algorithm have been described and validated for a wide range of applications [29,32,42–44]. For this problem of interest, depending on the applied conditions, the computational time for each run varies between 30 and 70 h and a parallel computer cluster.

III. RESULTS

The objective of this study is to understand the effects of pure oscillatory flows (zero net flow rate) on the dynamics of a liquid bridge inside microchannels. The discussion will start by analyzing the simple case of a stationary bridge located inside a microchannel. These results will be compared with literature and used for validating some of the parameters of the model. The complex physics of the nonstationary bridge under oscillatory flows will be then analyzed. To do so, both philic and phobic microchannels will be considered.

A. Stationary liquid bridge inside microchannels

A number of studies dealing with a captive stationary liquid bridge between or among solid particles have recently

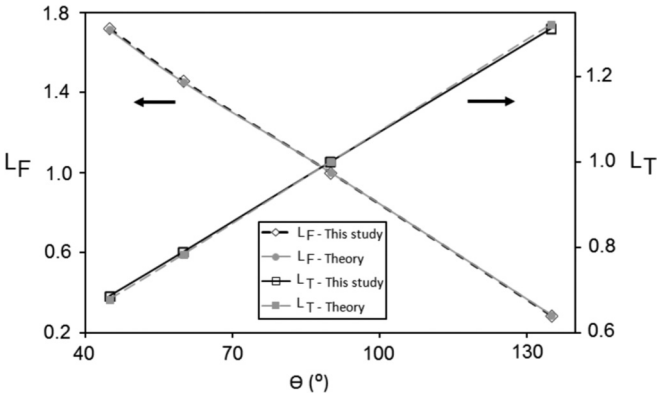

FIG. 2. Comparison of the footprint and throat lengths determined from the analytical expressions (gray) with those from the numerical simulations (black).

been carried out. In particular, Megias-Alguacil and Gauckler [45] analyzed the capillary forces between two small solid spheres bound by a convex liquid bridge. Assuming that in the stationary status the liquid bridge has a circular interface between two solid particles of the same size and using mathematical principles, the authors presented two simple expressions to determine the throat thickness and the principal radii of the liquid bridge. Adapting these expressions to the present system, dimensionless principal radii R, throat length L_T, and footprint length L_F have been obtained:

$$R = \frac{H}{W\cos(\theta)}, \tag{8}$$

$$L_T = 1+\frac{H}{W}\left(\frac{1}{\cos^2(\theta)}[\pi - 2\theta - \sin(2\theta)] - 2[1-\sin(\theta)]\right), \tag{9}$$

$$L_F = L_T + 2R[1-\sin(\theta)]. \tag{10}$$

In the above equations, θ is measured from inside the liquid bridge. The previous equations are valid when the solid substrate is philic to liquid bridge ($\theta < 90^\circ$), while for $\theta = 90^\circ$, the footprint and throat lengths are equal to 1. For phobic substrates, the equations are slightly different but can be obtained similarly using expressions for circular segments found in mathematical handbooks, e.g. [46].

The footprint and throat lengths of a liquid bridge inside a microchannel at different contact angles were determined using Eqs. (8)–(10) and the equivalent ones for phobic substrates. The results were compared with those obtained from our numerical model. Figure 2 depicts the results for $Cn = 10^{-2}$, $\Lambda = 10^{-2}$, $H_W = 1.25$, $L_W = 10.0$, and $\mathrm{Ca}_{\max} = 0.0$. It is clear that there is an excellent agreement between the numerical results and the analytical ones. This agreement was obtained as a result of a judicious choice of the parameters Cn and Λ. It should be noted that the chosen values are also in the range of those used in previous studies [9,44], which allow one to capture correctly the physics of the system. These values will be adopted in the remainder of the study.

The interfacial morphology developments of the liquid bridges from initial shape to the final stable equilibrium state in the absence of external flow ($\mathrm{Ca} = 0$, $f = 0$) are illustrated in Fig. 3. As the liquid bridge comes into contact with the solid substrate, it starts to adjust and reaches the final equilibrium state. For the philic case [Fig. 3(a)], as the liquid bridge starts to deform, the footprint becomes larger due to larger adhesive forces between the liquid and the solid. As a result of mass conservation, the throat gets thinner and finally once all forces are balanced the liquid bridge deformation stops. Opposite trends are observed in the phobic case [Fig. 3(b)]. It should be noted that in both cases there is no rupture or detachment of the liquid bridge from the substrate.

In what follows, first the physics of capillary bridges inside both philic and phobic microchannels subject to pure oscillatory flows (zero net flow) are analyzed. To do so, in addition to using two quantitative parameters, i.e., footprint (L_F) and throat length (L_T), the interfacial morphology development of the liquid bridge will be considered. Finally,

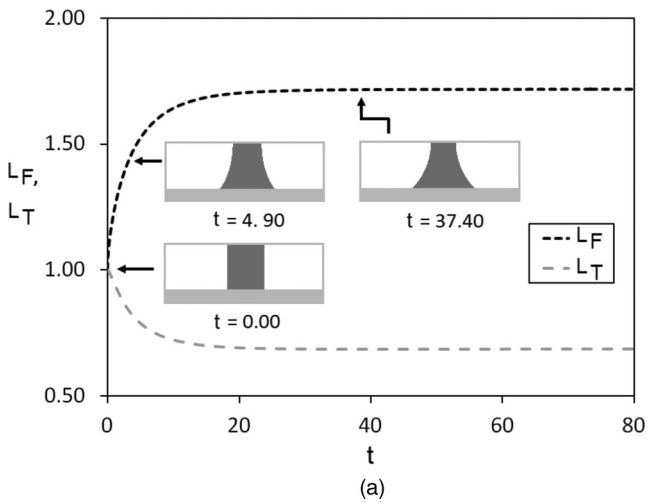

FIG. 3. Interfacial morphology development of the liquid bridges from initial shape to the final equilibrium stable state in the absence of external flow. (a) Contact angle $\theta = 45^\circ$. (b) Contact angle $\theta = 135^\circ$.

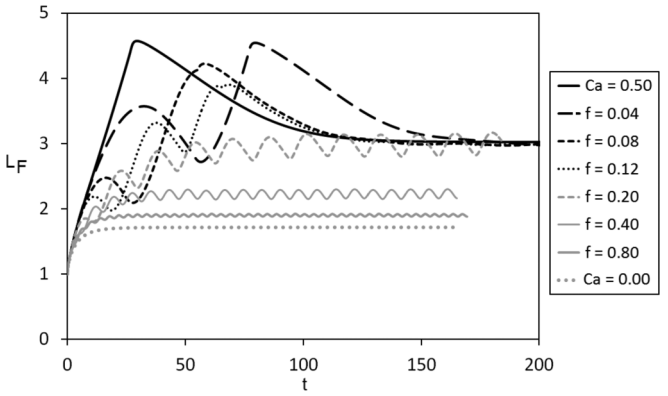

FIG. 4. Variations of the footprint length with time for different frequencies of the oscillatory flow: $Cn = 10^{-2}$, $\Lambda = 10^{-2}$, $H_W = 1.25$, $L_W = 10$, $\theta = 45^\circ$, and $\mathrm{Ca}_{\max} = 0.5$. Results of two constant flow rate cases, $\mathrm{Ca} = 0.5$ and $\mathrm{Ca} = 0.0$, are also included.

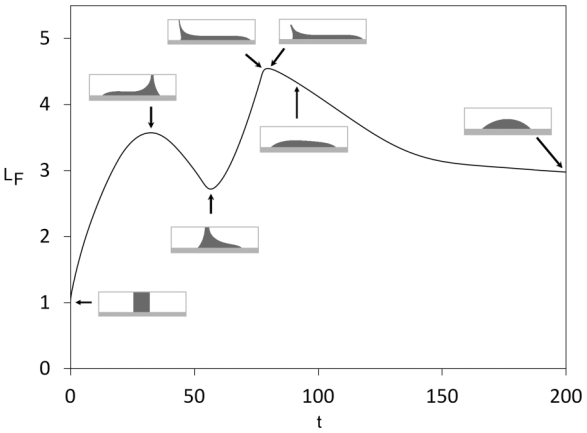

FIG. 6. Interfacial morphologies of the liquid bridge at different times for a frequency $f = 0.04$. All other parameters are the same as in Fig. 4.

we will explore whether the external flow velocity and liquid bridge are in phase or not and how to rationalize it.

B. Liquid bridge dynamics inside philic microchannels

Let's consider the case of a substrate that is philic to the liquid bridge, with $\theta = 45^\circ$. For the sake of brevity, the following parameters for the baseline model were chosen: $H_W = 1.25$; $L_W = 10$. Different fluid systems can be used as a reference for comparisons, but for the range of values examined in this study, a silicone fluid (e.g., 50 cSt silicone oil) -water system at ambient condition can be adopted as a possible benchmark. Note that in this system the surrounding fluid is water, and for this grade of silicone fluid, the viscosity ratio of silicone fluid to water M is approximately 50. It should be mentioned that due to the great variations in the viscosity of reservoir oil [47,48], silicone fluid-water systems are often used to understand multiphase flow dynamics in oil reservoirs [49–52].

Figures 4 and 5 show the variations of the footprint and throat with time for the stationary case ($\mathrm{Ca} = 0$, $f = 0$), oscillatory flows with six different frequencies ($\mathrm{Ca}_{\max} = 0.5, \overline{\mathrm{Ca}} = 0$) and a nonstationary displacement ($\mathrm{Ca} = \overline{\mathrm{Ca}} = 0.5, f = 0$). The latter scenario will be used for the purpose of comparisons between stationary ($\mathrm{Ca} = 0, f = 0$) and nonstationary ($\overline{\mathrm{Ca}} \neq 0$) systems.

Starting from the stationary case ($\mathrm{Ca} = 0$, $f = 0$), once the bridge comes into contact with the solid substrate, it starts to adopt itself to the wettability conditions. Thus it deforms symmetrically, and the footprint gets larger, while the throat gets thinner [Fig. 3(a)]. Finally, as a result of the force balance, the liquid bridge deformation stops and both the footprint and throat lengths reach rapidly a steady state.

In the case of the nonstationary displacement ($\mathrm{Ca} = 0.5, f = 0$), the bridge starts to deform and spreads on the solid substrate. As the interfaces deform, the spreading of the liquid increases due to larger liquid-solid adhesive forces (Fig. 4). This enhances viscous dissipation and as a result the bridge velocity on the surface decreases. Consequently, the rate of deformation in the throat section gets larger and the throat becomes thinner and ends up rupturing (Fig. 5).

Interesting trends are found once oscillatory flows with zero net flow rate come into play. In particular, it is found

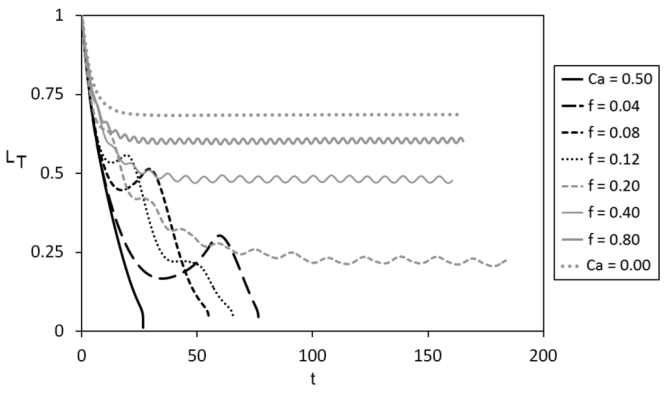

FIG. 5. Variations of the throat length with time for different frequencies of the oscillatory. The parameters are the same as in Fig. 4. Results of two constant flow rate cases, $\mathrm{Ca} = 0.5$ and $\mathrm{Ca} = 0.0$, are also included.

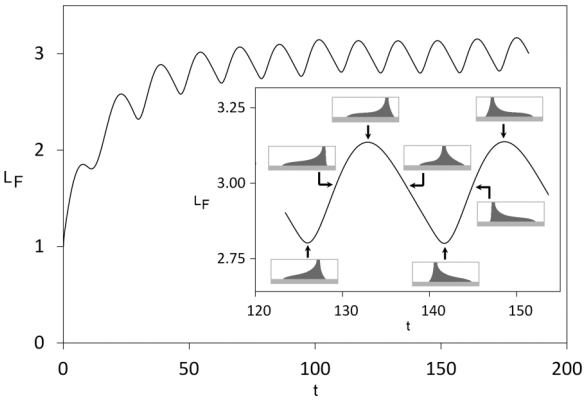

FIG. 7. Interfacial morphologies of liquid bridge at minimum, maximum, and average footprint lengths when periodic pattern of the liquid bridge motion is observed at $f = 0.20$. All other parameters are the same as in Fig. 4.

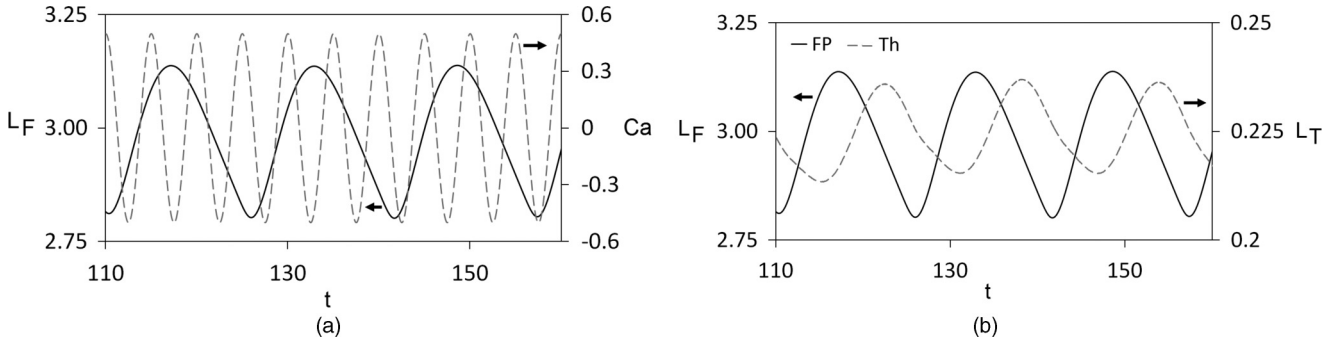

FIG. 8. Variations with time of (a) the footprint length and flow velocity Ca, and (b) the footprint and throat lengths for a frequency $f = 0.20$. All other parameters are the same as in Fig. 4.

that there is actually a bridge rupturing at low frequencies ($f = 0.04$–0.12); however, the rupture time and the footprint length at the time of rupture vary with the frequency. On the other hand, the bridge does not rupture at the high frequencies.

The trends for the throat lengths depicted in Fig. 5 reveal that for the frequencies that ultimately lead to rupture, the throat thickness goes through a series of oscillations before rupturing. The amplitude of the oscillation decreases with increasing f; however, the rupture time does not vary monotonically with the frequency. In particular, the rupture time for $f = 0.12$ falls in between those for $f = 0.04$ and $f = 0.08$. This special behavior may be explained by the nature of the deformation that the liquid goes through. For the lowest frequency $f = 0.04$, the length of the cycle of the oscillation is the longest but, as a result of the large amplitude of the deformation, the throat length cannot sustain the constriction of the second cycle and ends up rupturing (see movie Teta-45-F-004.avi in the Supplemental Material [53]). A similar sequence is observed for $f = 0.08$ and due to the large amplitude of the deformation, in this case too the bridge ruptures at the start of the second cycle which occurs earlier. The liquid bridge in the flow with $f = 0.12$ undergoes the same cycle; however, the amplitude of the deformation is not strong enough to lead to rupturing at the beginning of the second cycle, and the liquid bridge is able to survive through a full second cycle before breakup.

Further increase in the frequency results in oscillations of shorter cycle and smaller amplitudes. As a result the deformation and spreading of the liquid bridge is weakened to the extent that no rupturing occurs. In these cases, the throat and foot print lengths undergo perpetual motions that vary periodically with time. At large frequencies, the stabilizing effects get stronger and the bridge behavior approaches that of the stationary case (Ca $= 0$, $f = 0$). It is worth mentioning that the footprint length goes through trends similar to those observed in the case of the throat length, with a decrease in the amplitude and length of the cycle of oscillation with f. However, the fluctuations diminish faster with increasing frequency in the case of the footprint length. This is because of the viscous dissipation in the liquid-solid interfacial area.

Our numerical results indicate that flow oscillation affects four important aspects of the system; the available time for bridge deformation, the direction of the deformation, the magnitude of the spreading on the solid substrate, and the distance that the bridge slides on the substrate during each cycle. At low frequencies, changes in the flow direction are slow enough to allow the development of strong enough deformations that ultimately lead to the breakup of the bridge. The high frequencies, on the other hand, are not conducive for the development of large deformations and prevent any rupturing (see movie Teta-45-F-08.avi in the Supplemental Material [53]). This interpretation is confirmed by noting that

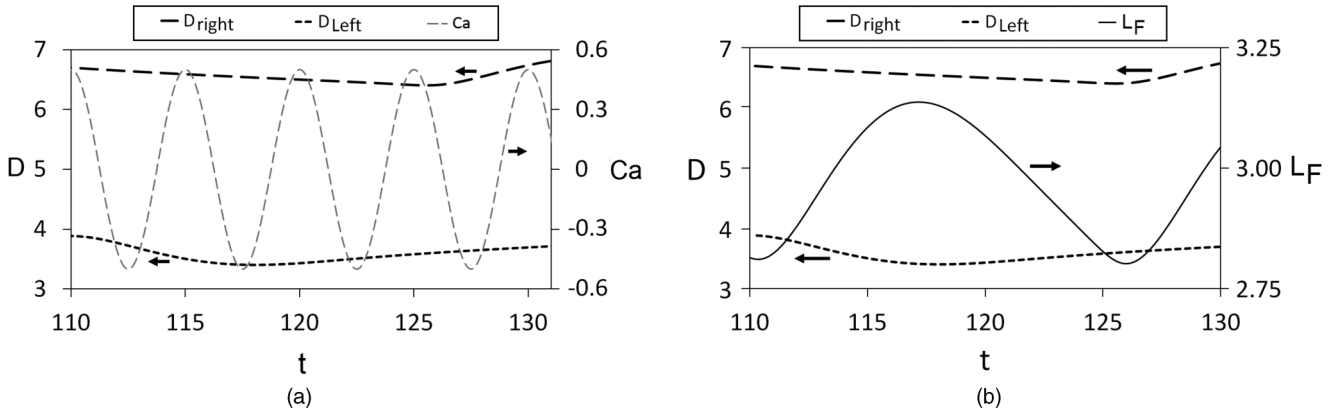

FIG. 9. (a) Variations of the flow velocity Ca, and (b) the footprint L_F, when positions of the left and right contact lines D on the solid substrate change. The frequency f is 0.20, and other parameters are the same as in Fig. 4.

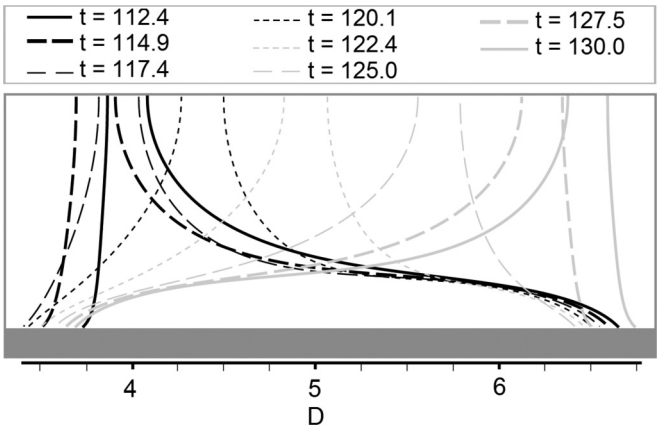

FIG. 10. Interfacial morphology of the liquid bridge and the positions of the contact lines at times when the absolute magnitude of the velocity is maximum. The frequency f is 0.20, and other parameters are the same as in Fig. 4.

the maximum footprint is larger and the rupturing occurs earlier in the case of the constant nonstationary flow (Ca $=$ $0.5, f = 0$), where the flow does not experience any change in direction. It is important to note that, in these inertialess computations, at least in the range of the studied frequencies, we did not observe mean flow. This is attributed to the dominance of the viscous forces which dissipate the flow energy.

To further understand the mechanisms behind the different reported behaviors, interfacial morphological developments are presented in Figs. 6 and 7 for a case resulting in rupture and one where no breakup occurs. As it can be seen from Fig. 6 for the rupturing case ($f = 0.04$), once the liquid bridge ruptures from the middle point at $t \approx 80$, it leaves a sessile drop on each plate. Theses drops then adapt themselves to the flow by retracting and starting to slide in an oscillatory motion on the solid substrate. However, the fluctuation in the footprint length is negligible and hence is not reflected in the variations of the footprint length depicted in Fig. 6. These very small

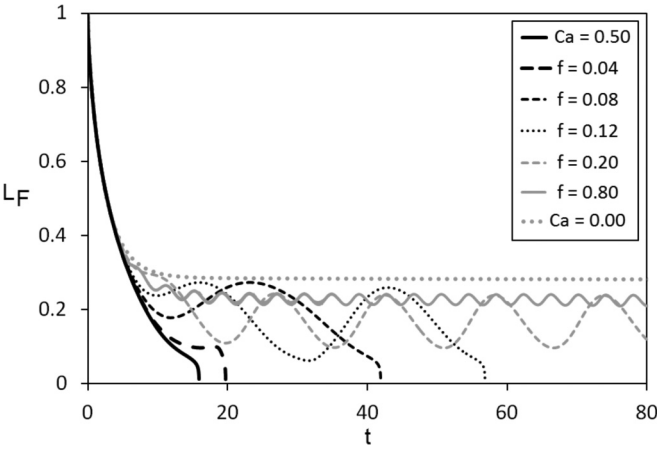

FIG. 11. Variations of the footprint length with time for different frequencies of the oscillatory flow rate when $\theta = 135^\circ$. All other parameters are the same as in Fig. 4. Results of two constant flow rate cases, Ca $= 0.5$ and Ca $= 0.0$, are also included.

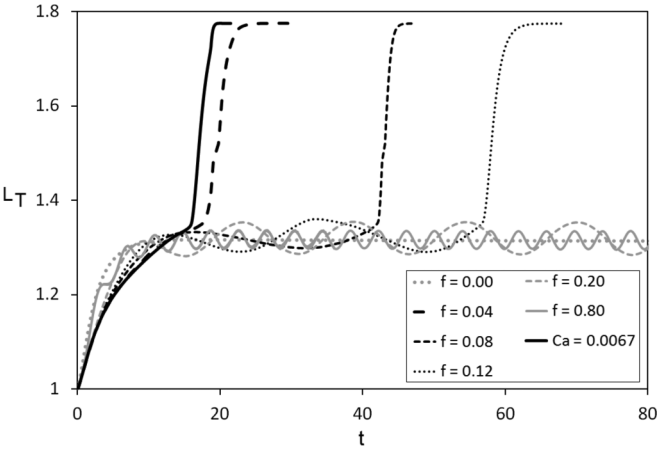

FIG. 12. Variations of the throat length with time for different frequencies of the oscillatory flow rate when $\theta = 135^\circ$. All other parameters are the same as in Fig. 4. Results of two constant flow rate cases, Ca $= 0.5$ and Ca $= 0.0$, are also included.

fluctuations are the direct result of the large reduction of the imposed forces (shear, normal, and pressure force [44]) on the created drops on the philic substrates which do not get affected significantly by the oscillations in flow magnitude and direction.

Interesting trends are found in the case of an oscillatory nonrupturing liquid bridge at, e.g., $f = 0.20$. In Fig. 7, close snapshots of the liquid bridge interfacial morphologies are shown when the steady periodic regime is reached. Let's consider $t \approx 125$, where the footprint length approaches its minimum. At this minimum point, the liquid bridge throat is located towards the right. In the subsequent stage where the footprint length increases from its minimum value to the maximum one, the position of the throat remains virtually unchanged. Once the footprint length goes past its maximum value and starts decreasing, the throat starts to move towards the left and reaches its middle position when the footprint length is at its average value. The throat finally approaches the left side when the footprint reaches its minimum.

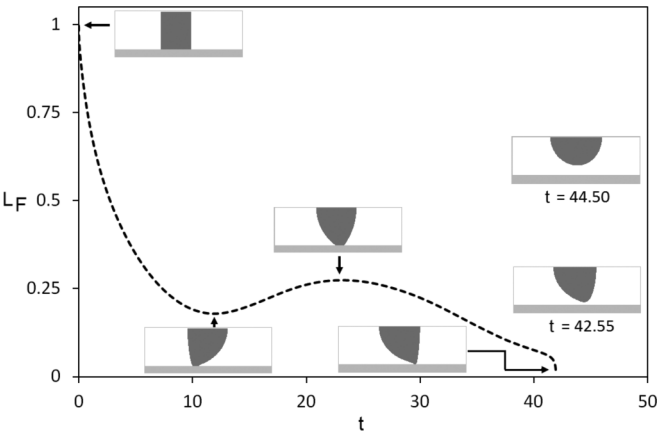

FIG. 13. Interfacial morphology of the liquid bridge at different times for $\theta = 135^\circ$ and $f = 0.08$. All other parameters are the same as in Fig. 4.

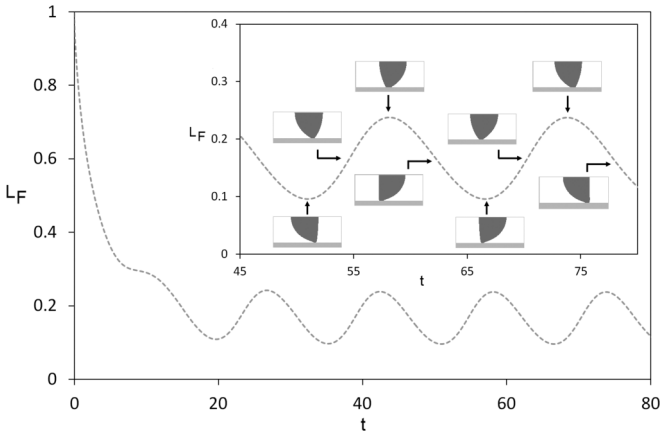

FIG. 14. Interfacial morphology of the liquid bridge at different times for $\theta = 135^\circ$ and $f = 0.20$. All other parameters are the same as in Fig. 4.

This qualitative description indicates that the oscillatory behaviors of the throat, footprint, and flow are not in phase. This out-of-phase behavior is clear from Fig. 8 depicting the variations with time of the footprint and throat lengths as well as the injection velocity (Ca). As the trends show, not only is the velocity out of phase with the footprint and throat lengths but the footprint and throat also show a phase difference. These phase differences can be attributed to the fact that the response of the liquid bridge to the flow field is controlled by the motion of the two (left and right) contact lines on the solid substrates and the deformation of the two fluid-fluid interfaces.

To confirm the previous justification, the variations of the dimensionless distances of the left (D_{left}) and right (D_{right}) contact lines on the solid substrate measured from the left side of the computational domain are shown in Fig. 9 for $110 < t < 130$. At $t = 110$, the left contact line moves towards the left (D_{left} is reduced); in the same time the right contact line also moves in the same direction. However, when D_{left} reaches its minimum ($t \approx 117$) and then starts to increase (left contact line move towards the right), the right contact line still continues to move towards the left. These differences in the contact lines' movements are the result of competitions between viscous dissipation on the solid substrate, external flow induced forces on the liquid bridge, interfacial deformation, and the distance between the two contact lines. Hence the contact lines do not always move in the same direction.

For further analysis, interfacial morphology of the liquid bridge and the positions of the contact lines D are presented in Fig. 10. The trends are shown for times when the absolute magnitude of the flow velocity reaches its maximum. As Fig. 10 indicates and as discussed, the left and right contact lines may move towards different directions at extrema points of the velocity. Meanwhile, the fluid-fluid interfaces can also have different shapes at different extrema of the flow velocity. As it is clear from Fig. 10, the positions of the contact lines on the solid substrate do not experience much changes compared to the fluid-fluid interfaces in the throat region where the flow velocity is the largest. This is because of the large viscous dissipation in the liquid-solid interfacial area. Moreover, it should be noted that even though the throat experiences more deformation as a result of this viscous dissipation, the variation in the footprint length L_F is much larger than that in the throat length L_T.

C. Liquid bridge dynamics inside phobic microchannels

It is known that the wall wettability properties change the solid-liquid interfacial area and affect the hydrodynamic forces. This in turn affects not only the footprint and throat lengths but also changes the distance that the liquid bridge slides freely on the solid substrate. To explore the effects of the wettability, a microchannel with phobic walls of contact angle $\theta = 135^\circ$ is considered.

Figures 11 and 12 depict the variations with time of the footprint and throat lengths for the same parameters as those in Fig. 4, except for the fact that the substrate is now phobic, $\theta = 135^\circ$.

In the case of the nonstationary flow ($\text{Ca} = 0.5, f = 0.0$), as soon as the liquid bridge adapts itself to the phobic surface the footprint gets smaller than the throat because of depletion forces between the solid and liquid. In these conditions the liquid bridge will detach from the surface as a response to the forces imposed by higher external flow rate and small viscous dissipation. Unlike the philic substrate, rupturing is replaced with detachment from the phobic surface.

This detachment is also observed in the oscillatory cases at low frequencies (see movie Teta-135-F-004.avi in the Supplemental Material [53]). In these cases, the bridge detaches from the substrate as a result of the smaller viscous dissipation on the solid and slow changes in the flow direction. However, in contrast with the rupturing time in the philic case, the

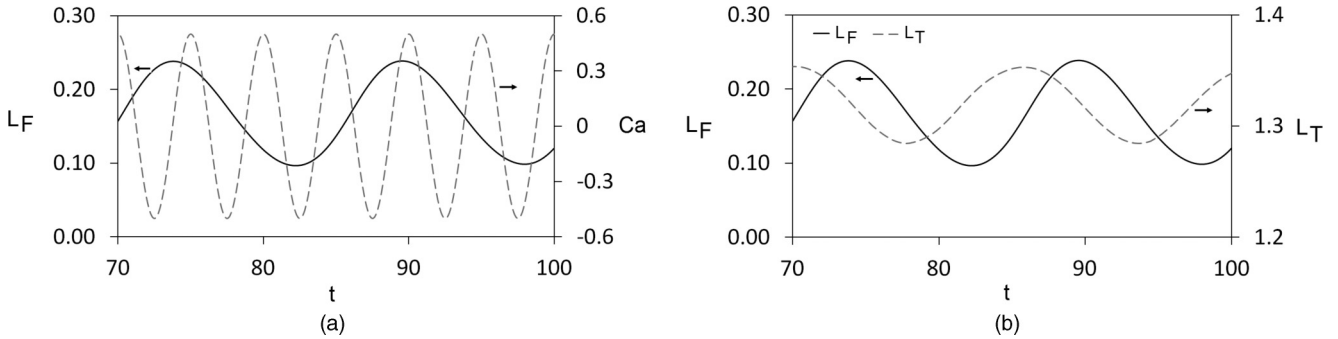

FIG. 15. Variations with time of (a) the footprint length and flow velocity Ca, and (b) the footprint and throat lengths for a frequency $f = 0.20$ and $\theta = 135^\circ$. All other parameters are the same as in Fig. 4.

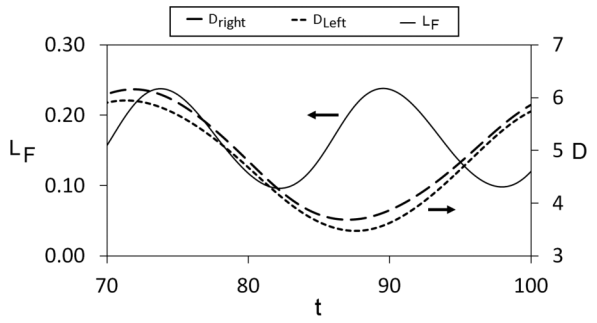

FIG. 16. Variations of the footprint length and position of the left and right contact lines on the solid substrate, for a frequency $f = 0.20$ and $\theta = 135^\circ$. All other parameters are the same as in Fig. 4.

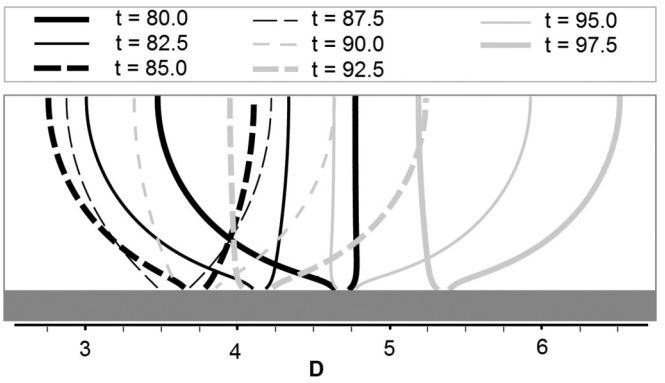

FIG. 17. Interfacial morphology of the liquid bridge and the positions of the contact lines at times when the absolute magnitude of the velocity is maximum. Contact angle θ and frequency f are 135° and 0.20, respectively. All other parameters are the same as in Fig. 4.

detachment time shows a monotonic increase with increasing frequency.

Similar to the philic substrate, detachment is replaced with a stabilized periodic pattern in the liquid bridge motion at higher frequencies, and approaches the limit case of the resting state (Ca = 0, $f = 0$) at very high frequencies (see movie Teta-135-F-08.avi in the Supplemental Material [53]). It is, however, worth noting that the throat length for a phobic substrate actually oscillates around that of the resting case and exhibits much smaller deviations from it in comparison with the philic substrate. This is mainly due to the stronger deformations of the liquid bridge and its spreading on the surfaces between philic plates.

Morphological developments of the liquid bridge between phobic parallel plates at two frequencies ($f = 0.08$ and $f = 0.2$) are shown in Figs. 13 and 14. In the case that results in detachment, the bridge separates from the surface after one cycle and forms a drop that starts to oscillate in response to the oscillatory flow (Fig. 13). As mentioned earlier this is because of lower viscous dissipation between solid-liquid and slow change in flow direction, which provides enough time for the liquid bridge to experience more deformation and detach from the solid wall. On the other hand, for the high frequency, the liquid bridge ends in a perpetual periodic motion between the plates (Fig. 14) as a direct result of less deformation because of time shortage. Like the case involving philic surfaces, the flow velocity, footprint, and throat lengths variations in time are out of phase (Fig. 15). However, between parallel phobic plates, variation in footprint length L_F is comparable with variation in the throat length L_T.

It is worth mentioning that the phobicity induces significant effects that decrease this difference between the footprint and the velocity field. Mutual effects of the contact lines on the substrate on each other are stronger due to the shorter distance that separates them. As a result, the contact lines tend to move virtually in phase (same direction) as shown in Fig. 16.

Interfacial morphology of the liquid bridge and the positions of the contact lines at the times that the flow velocity reaches its extrema are depicted in Fig. 17. Generally speaking, the throat region does not experience large deformations. This is in contrast to what was reported in the case of the philic walls. The main reason for this is the fact that the footprint length of the liquid bridge inside the philic microchannel is larger compared to the phobic one, while the throat section is thinner. On the other hand, between phobic plates, the contact lines on the solid substrate move longer distances because of lower viscous dissipation.

IV. CONCLUSION

A comprehensive investigation of the dynamics of liquid bridges inside straight 2D microchannels in the presence of an external oscillatory flow field has been carried out. The velocity field was chosen such that the net flow rate is zero, and hence is similar to a stationary case. The results indicate that, depending on the substrate wettability properties and frequency level, the bridge may rupture, detach, or show a perpetual time periodic oscillatory motion between the plates.

For small enough frequencies of the flow velocity, the liquid bridge ruptures in the case of a philic microchannel wall and the rupturing time does not follow a monotonic trend with the frequency. For phobic plates, rupturing is replaced by detachment at small frequencies, except that in contrast to the philic walls' scenario, the detachment time increases monotonically with increasing frequency.

On the other hand, regardless of the plates wettability properties, increasing the frequency results in stabilization effects and a behavior approaching that of the stationary system where no rupture or detachment can be observed. This stable behavior is the direct result of less deformation of the liquid bridge due to the fast flow direction change and motion of contact lines on the solid substrate. Furthermore, it was found that the flow velocity is out of phase with the footprint and throat lengths and that the latter two also show a phase difference. These differences were attributed to the motion of the two contact lines on the solid substrates and the deformation of the two fluid-fluid interfaces.

These results are to be contrasted with the corresponding stationary case where neither detachment nor rupture can be observed, regardless of the wetting properties of the substrate. They also reveal that, for the same zero net injection flow rate (pure oscillatory flow), it is possible to control the dynamics of the liquid bridge through the frequency of the flow velocity. Rupturing or detachment can be induced with frequencies lower than a critical value f_c. Even though the results are presented for fixed flow and geometry parameters, it

is expected that f_c will depend on the flow properties, viscosity ratio, wettability property, and geometry characteristics.

It is expected that the results of this fundamental research will contribute to advancing our understanding of the dynamics of liquid bridges in confined pathways, and will help in the future design and optimization of processes in conventional or modern applications such as enhanced oil recovery, microfluidics, and lab-on chips devices.

ACKNOWLEDGMENTS

The authors would like to thank B. Eckhardt (Associate Editor) and anonymous reviewers for their constructive comments and suggestions. The authors also acknowledge financial support of NSERC/AERI (AIEES)/Foundation CMG and iCORE (AITF) Chairs Funds and the use of the computing resources of the WestGrid cluster.

[1] C. M. Marle, *Multiphase Flow in Porous Media* (Editions Technip, Paris, 1981).
[2] R. Lenormand, E. Touboul, and C. Zarcone, J. Fluid Mech. **189**, 165 (1988).
[3] T. Y. Chen, J. A. Tsamopoulos, and R. J. Good, J. Colloid Interface Sci. **151**, 49 (1992).
[4] T. Y. Chen and J. A. Tsamopoulos, J. Fluid Mech. **255**, 373 (1993).
[5] M.-H. Meurisse and M. Querry, J. Tribol. **128**, 575 (2006).
[6] J. H. Nam and M. Kaviany, Int. J. Heat Mass Transf. **46**, 4595 (2003).
[7] C.-Y. Wang, Chem. Rev. **104**, 4727 (2004).
[8] F. Y. Zhang, X. G. Yang, and C. Y. Wang, J. Electrochem. Soc. **153**, A225 (2006).
[9] M. Ahmadlouydarab, Z.-S. Liu, and J. J. Feng, Int. J. Multiphase Flow **47**, 85 (2012).
[10] E. B. Dussan V., Annu. Rev. Fluid Mech. **11**, 371 (1979).
[11] X. Zhang, R. S. Padgett, and O. A. Basaran, J. Fluid Mech. **329**, 207 (1996).
[12] A. Ramos, F. Garcia, and J. M. Valverde, Eur. J. Mech. B/Fluids **18**, 649 (1999).
[13] O. Pitois, P. Moucheront, and X. Chateau, J. Colloid Interface Sci. **231**, 26 (2000).
[14] S. Dodds, Ph.D. thesis, University of Minnesota, 2011.
[15] J. M. Haynes, J. Colloid Interface Sci. **32**, 652 (1970).
[16] M. A. Erle, R. D. Gillette, and D. C. Dyson, Chem. Eng. J. **1**, 97 (1970).
[17] M. J. Russo and P. H. Steen, J. Colloid Interface Sci. **113**, 154 (1986).
[18] F. M. Orr, L. E. Scriven, and A. P. Rivas, J. Fluid Mech. **67**, 723 (1975).
[19] W. C. Carter, Acta Metall. **36**, 2283 (1988).
[20] D. J. Molot, J. Tsamopoulos, T. Y. Chen, and N. Ashgriz, J. Fluid Mech. **255**, 411 (1993).
[21] A. Valencia, M. Brinkmann, and R. Lipowsky, Langmuir **17**, 3390 (2001).
[22] N. Ichikawa, M. Kawaji, and M. Misawa, J. Jpn. Soc. Micrograv. Appl. **20**, 292 (2003).
[23] J. Nicolas, D. Rivas, and J. Vega, J. Fluid Mech. **354**, 147 (1998).
[24] M. Kawaji, M. Nasr-Esfahany, and R. Liang, Surf. Tens.-Driven Flows Appl. **2006**, 75 (2006).
[25] R.-Q. Liang and M. Kawaji, Chin. Rev. Lett. **31**, 044701 (2014).
[26] A. K. Gunstensen and D. H. Rothman, J. Geophys. Res. **98**, 6431 (1993).
[27] H. Li, C. Pan, and C. T. Miller, Phys. Rev. E **72**, 026705 (2005).
[28] A. G. Yiotis, J. Psihogios, M. E. Kainourgiakis, A. Papaioannou, and A. K. Stubos, Colloids Surf. A: Physicochem. Eng. Aspects **300**, 35 (2007).
[29] M. Ahmadlouydarab, Z.-S. Liu, and J. J. Feng, Int. J. Multiphase Flow **37**, 1266 (2011).
[30] D. Jacqmin, J. Fluid Mech. **402**, 57 (2000).
[31] P. Yue, J. J. Feng, C. Liu, and J. Shen, J. Fluid Mech. **515**, 293 (2004).
[32] P. Yue, C. Zhou, J. J. Feng, C. F. Ollivier-Gooch, and H. H. Hu, J. Comput. Phys. **219**, 47 (2006).
[33] I. S. Goldenberg, G. F. Carey, R. Mclay, and L. Phinney, Int. J. Numer. Methods Fluids **11**, 87 (1990).
[34] A. Sinclair, Ph.D. thesis, University of New South Wales, 2012.
[35] R. Raju and R. Mittal, AIAA Pap. **2005**, 4751 (2005).
[36] R. Y. Chen, J. Fluids Eng. **95**, 153 (1973).
[37] B. Atkinson, M. Brocklebank, C. Card, and J. Smith, AIChE J. **15**, 548 (1969).
[38] P. Yue, C. Zhou, and J. J. Feng, J. Fluid Mech. **645**, 279 (2010).
[39] P. Yue and J. J. Feng, Phys. Fluids **23**, 012106 (2011).
[40] P. Gao and J. J. Feng, Phys. Fluids **21**, 102102 (2009).
[41] P. Gao and J. J. Feng, J. Fluid Mech. **668**, 363 (2011).
[42] P. Gao and J. J. Feng, J. Fluid Mech. **682**, 415 (2011).
[43] C. Zhou, P. Yue, J. J. Feng, C. F. Ollivier-Gooch, and H. H. Hu, J. Comput. Phys. **229**, 498 (2010).
[44] M. Ahmadlouydarab and J. J. Feng, J. Fluid Mech. **746**, 214 (2014).
[45] D. Megias-Alguacil and L. J. Gauckler, Powder Technol. **198**, 211 (2010).
[46] J. W. Harris and H. Stocker, *Handbook of Mathematics and Computational Science* (Springer-Verlag, New York, 1998).
[47] A. Hemmati-Sarapardeh, M. Khishvand, A. Naseri, and A. H. Mohammadi, Chem. Eng. Sci. **90**, 53 (2013).
[48] H. P. Rønningsen, Energy Fuels **7**, 565 (1993).
[49] L. K. Abidoye and D. B. Das, Adv. Water Res. **74**, 212 (2014).
[50] M. Stöhr, K. Roth, and B. Jähne, Exp. Fluids **35**, 159 (2003).
[51] O. I. Frette, K. J. Maløy, J. Schmittbuhl, and A. Hansen, Phys. Rev. E **55**, 2969 (1997).
[52] I. Okamoto, S. Hirai, and K. Ogawa, Meas. Sci. Technol. **12**, 1465 (2001).
[53] See Supplemental Material at http://link.aps.org/supplemental/10.1103/PhysRevE.91.023002 for the interfacial development of the liquid bridge inside both philic and phobic microchannels.